ARMY RESEARCH LABORATORY

Advanced Suspension and Control Algorithm for U.S. Army Ground Vehicles

by Muthuvel Murugan and Ross Brown

ARL-TR-6415 **April 2013**

NOTICES

Disclaimers

The findings in this report are not to be construed as an official Department of the Army position unless so designated by other authorized documents.

Citation of manufacturer's or trade names does not constitute an official endorsement or approval of the use thereof.

Destroy this report when it is no longer needed. Do not return it to the originator.

Army Research Laboratory
Aberdeen Proving Ground, MD 21005-5069

ARL-TR-6415 **April 2013**

Advanced Suspension and Control Algorithm for U.S. Army Ground Vehicles

Muthuvel Murugan
Vehicle Technology Directorate, ARL

Ross Brown
Motile Robotics Inc.

REPORT DOCUMENTATION PAGE	Form Approved OMB No. 0704-0188

1. REPORT DATE *(DD-MM-YYYY)*	2. REPORT TYPE	3. DATES COVERED (From - To)
April 2013	Final	2011–2012

4. TITLE AND SUBTITLE
Advanced Suspension and Control Algorithm for U.S. Army Ground Vehicles

5a. CONTRACT NUMBER

5b. GRANT NUMBER

5c. PROGRAM ELEMENT NUMBER

6. AUTHOR(S)
Muthuvel Murugan and Ross Brown*

5d. PROJECT NUMBER

5e. TASK NUMBER

5f. WORK UNIT NUMBER

7. PERFORMING ORGANIZATION NAME(S) AND ADDRESS(ES)
U.S. Army Research Laboratory
ATTN: RDRL-VTM
Aberdeen Proving Ground, MD 21005-5069

8. PERFORMING ORGANIZATION REPORT NUMBER
ARL-TR-6415

9. SPONSORING/MONITORING AGENCY NAME(S) AND ADDRESS(ES)

10. SPONSOR/MONITOR'S ACRONYM(S)

11. SPONSOR/MONITOR'S REPORT NUMBER(S)

12. DISTRIBUTION/AVAILABILITY STATEMENT
Approved for public release; distribution is unlimited.

13. SUPPLEMENTARY NOTES
*Motile Robotics Inc., 1809 Fashion Ct., Ste. 107, Joppa, MD 21085

14. ABSTRACT
This report documents the research study conducted on advanced suspension and control algorithms for U.S. Army ground vehicles. It is extremely important to isolate the vehicle body and its contents from terrain-induced vibrations. This enhancement will provide our Warfighters a less-disruptive environment, enabling them to improve their operational effectiveness. Reduced vibration enabled through a well-designed suspension system with an efficient control algorithm will permit higher vehicle speeds as well as better target-aiming accuracy in theater. Military vehicles with a high center of gravity and large variations in gross weights can greatly benefit by using advanced suspension technologies with active, adaptive preview-sensor-based control algorithms. The objective of this research study is to develop a preview-sensor-based control algorithm that can effectively work with advanced semi-active dampers, such as the magnetorheological fluid damper. This report provides a record of the research findings from this research project on advanced suspension and control algorithms for Army ground vehicles.

15. SUBJECT TERMS
advanced suspension, control algorithms, vehicle dynamics, semi-active damper, vibration control

16. SECURITY CLASSIFICATION OF:			17. LIMITATION OF ABSTRACT	18. NUMBER OF PAGES	19a. NAME OF RESPONSIBLE PERSON
a. REPORT	b. ABSTRACT	c. THIS PAGE			Muthuvel Murugan
Unclassified	Unclassified	Unclassified	UU	38	19b. TELEPHONE NUMBER (*Include area code*) 410-278-7903

Standard Form 298 (Rev. 8/98)
Prescribed by ANSI Std. Z39.18

Contents

List of Figures

List of Tables

Acknowledgments

The authors thank Mr. Marcus Mazza, U.S. Army Materiel Systems Analysis Activity (AMSAA), for his assistance and guidance in building a multibody vehicle dynamics model of a typical light tactical Army vehicle, such as a modified HMMWV (High-Mobility Multipurpose Wheeled Vehicle) model. The authors also thank Dr. Norman Wereley, Professor of Aerospace Engineering at the University of Maryland, College Park, MD, for developing a fail-safe magnetorheological suspension damper that can be used for verification and validation of control algorithms on a quarter-car representative suspension test rig. In addition, the authors thank Dr. Jin Yoo, U.S. Army Research Laboratory, Vehicle Technology Directorate, for his help assembling the advanced quarter-car suspension test rig, and Dr. Peilin Song, AMSAA, for his suggestions in the dynamics modeling and simulation activities.

INTENTIONALLY LEFT BLANK.

1. Summary

The ground vehicle suspension system has a very strong influence on the handling, stability, ride, and durability characteristics of a vehicle as it negotiates different types of terrains. Therefore, research advancements in suspension and control system technologies are needed to innovate better systems, which are compact, self-powered, easily adaptable, and tunable to different vehicle weight configurations and different terrain types. Military ground vehicles with high a center of gravity and large variations in gross weights can greatly benefit by using advanced suspension technologies with active, adaptive, preview-sensor-based control algorithms. The ultimate objective of this research work is to develop a preview-sensor-based nonlinear control algorithm that can effectively work with semi-active dampers, such as the magnetorheological (MR) fluid damper. This research study attempts to develop advanced suspension technology with active, adaptive control algorithms using dynamics simulation tools and then validate them experimentally to demonstrate the desired effectiveness by reducing vehicle body acceleration by 10% or increasing off-road speed by 10%. This report discusses and summarizes the research activities conducted by the U.S. Army Research Laboratory, Vehicle Technology Directorate (ARL-VTD). The main tasks of this research, to be accomplished over a span of two years, are as follows:

- Develop and adapt generalized predictive control algorithms and extend them to include nonlinear system identification for use with MR dampers.
- Characterize performance of developed control algorithms and select the optimum algorithm based on simulation using a quarter-car suspension system and multibody vehicle dynamics models.
- Determine effectiveness of control algorithms based on the ability to control vibration caused by terrain disturbances, as well as overall vehicle handling and ride performance.
- Leverage ARL broad agency agreement (BAA) research with the University of Maryland to develop an advanced prototype MR damper that can verify the effectiveness of control algorithms using a quarter-car representative 2-degree-of-freedom (2-DOF) Advanced Suspension Test Rig (ASTR) being currently installed at ARL-VTD's laboratory.
- Build test setup and characterize baseline and advanced MR dampers on quarter-car representative ASTR. Conduct verification and validation of control algorithms to assess their vibration control effectiveness.

This report specifically covers the tasks conducted during the first year of research to develop an advanced semi-active suspension system and adaptive control algorithms for improving vehicle vibration control and ride quality of military ground vehicles.

2. Introduction

Passive suspension systems for Army wheeled vehicles are optimized for passenger comfort and road/terrain handling qualities. These two goals often lead to conflicting design requirements. With a view toward designing suspension systems that would improve both performance metrics, ARL-VTD has underway a research program aimed at developing active suspension systems for implementation on the next generation of Army vehicles. The overall objective is to reduce vibration-induced fatigue as well as improve target aiming precision in theater.

There are basically two main groups of active suspension systems: semi- and fully active. Semi-active suspension systems vary spring and damper properties to add or remove energy from the system according to some applied control algorithm. Usually, this is achieved through variable damping components, such as variable orifice valves or MR fluids. Fully active suspension systems use force actuators to add and remove energy from the system. This function can be achieved using hydraulic, pneumatic, or electromechanical actuators. Current research at VTD is addressing both types of systems.

The generalized predictive control (GPC) algorithm is a linear, time-invariant, multi-input/multi-output method that uses an AutoRegressive eXogenous (ARX) model to represent the input-output behavior of the system and to design the controller (*1–4*). Three variants of the techniques have been evaluated. In the first variant, no explicit account is taken of the disturbances acting on the system during system identification and controller design (*2*, *3*). This version is called GPC With Implicit Disturbance in this report. The second and third variants take explicit account of measurable disturbances. The first of these two (called GPC With Explicit Disturbance herein) uses only the past values of the measured disturbances, while the latter (called GPC With Preview in this report) additionally uses measurements (or predictions) of future disturbances (*1*, *4*).

This report discusses the control methodology of GPC algorithms, vehicle dynamics models and co-simulation with control algorithms, extension of GPC to enable nonlinear capability, advanced MR damper development, and 2-DOF suspension test rig assembly and setup. The report finishes with some concluding remarks on the results of the completed research activities and some comments on the nature of some planned future work.

3. Vehicle Dynamics Model

TruckSim is a widely used, commercially available software tool used to simulate and analyze the dynamic behavior of wheeled vehicles. It is employed in conjunction with Matlab/Simulink to simulate the effects of control algorithms on a full-vehicle model. The TruckSim model takes the full vehicle and terrain into consideration, including driver controls and steering, road geometry, suspensions, tires, and power train. Component parameters are input into TruckSim via constants, linear coefficients, nonlinear tables, and algebraic formulae.

Full three-dimensional road geometry was specified at 0.1-m increments in this research work. The steering system captures the steer of each wheel due to the steering system geometry and compliances. The suspension system models capture the full nonlinear kinematical behaviors and compliances of the front and rear suspensions. These models include data for springs, dampers, and jounce/rebound stops. The tire model is an internal table-based, single-point contact model. Nonlinear tables using actual measured tire data represent vertical force, lateral force, longitudinal force, aligning moment, and overturning moment as functions of deflection, slip, load, and camber. The power-train model includes engine torque, torque convertor characteristics, and transmission gear ratios and efficiencies. A representative TruckSim tactical vehicle model (modified High-Mobility Multipurpose Wheeled Vehicle [HMMWV] model) that was developed in collaboration with the U.S. Army Materiel Systems Analysis Activity (*5*) is shown in figure 1. Figure 2 contains a graphical layout of the suspension as modeled in SuspensionSim that works with TruckSim software.

Figure 1. TruckSim-modified HMMWV model on Perryman3.

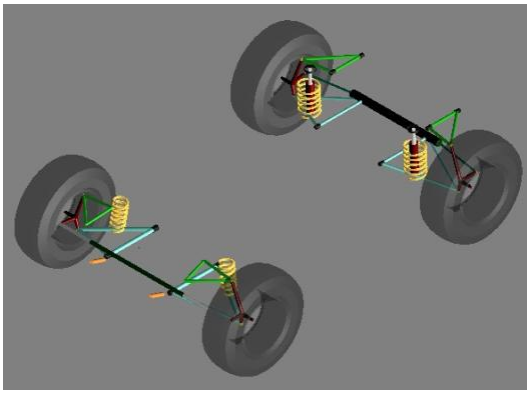

Figure 2. Representative HMMWV suspension model.

For this research, we modified some of the basic HMMWV vehicle parameters to study the performance of GPC algorithms on various terrain profiles. The vehicle mass was doubled. The suspension springs were stiffened, and the front damping coefficient was reduced. This is shown in table 1.

Table 1. Vehicle parameters for modified HMMWV model.

Parameter	Basic HMMWV	Modified HMMWV
Sprung mass	2210 kg	5000 kg
Front spring	150 N/mm	250 N/mm
Front damper	30 kNs/m	15 kNs/m
Rear spring	150 N/mm	400 N/mm
Rear damper	30 kNs/m	30 kNs/m

4. Control Algorithm Methodology

The steps in developing a GPC-based controller are system identification and derivation of the control law. System identification is based on the derivation of a multistep output prediction equation using the observer Markov parameters (OMPs) that comprise the ARX model used to characterize the system. The control law then follows from the minimization of a quadratic performance equation involving the predicted response and the control command. A summary of the key steps of the process, adapted from the more extensive development present in Kvaternik et al. (*4*), is given next. Since GPC is a multi-input/multi-output controller, the control command,$\{u_t\}$, measured response,$\{y_t\}$, and external disturbance, $\{d_t\}$, can be vectors whose elements correspond to the values of a specific actuator or sensor at time *t*.

4.1 GPC With Implicit Disturbance

The relationship between the input and output time histories of a linear time-invariant multi-input/multi-output system can be described by an ARX model of the form

$$\begin{aligned} y(t) = \alpha_1 y(t-1) + \alpha_2 y(t-2) + \ \ldots + \alpha_p y(t-p) \\ + \beta_0 u(t) \ + \beta_1 u(t-1) + \ \ldots + \beta_p u(t-p) \end{aligned} \quad . \tag{1}$$

This equation says that the output, *y(t)*, at the current time step, *t*, may be estimated by using *p* sets of the previous input and output measurements, *u(t-1), …, u(t-p), y(t-1),…,y(t-p)*, and the current input, *u(t)*. The integer *p* denotes the order of the ARX model. The coefficient matrices α_i and β_i are called observer Markov parameters and are the quantities computed by the identification process (*6*).

To start the identification process, the system is excited with band-limited white noise. These independent random excitations are applied concurrently to all of the r_c control inputs. The r_c control inputs and the *m* response outputs are recorded for *L* samples. The resulting input and output time histories, *u* and *y*, are then used to form the data matrices *y* and *V*.

$$\boldsymbol{y} = \bar{\boldsymbol{Y}}\boldsymbol{V} \ , \tag{2}$$

where

$$\underset{\boldsymbol{m}\ \mathbf{x}\ \boldsymbol{L}}{\boldsymbol{y}} = [\boldsymbol{y_0} \quad \cdots \quad \boldsymbol{y_{L-1}}] \tag{3}$$

and

$$\underset{[\boldsymbol{r_c} + (\boldsymbol{r_c} + \boldsymbol{m})\boldsymbol{p}]\ \mathbf{x}\ \boldsymbol{L}}{\boldsymbol{V}} = \begin{bmatrix} \boldsymbol{u_0} & \boldsymbol{u_1} & \boldsymbol{u_2} & \cdots & \boldsymbol{u_p} & \cdots & \boldsymbol{u_{L-1}} \\ & \boldsymbol{u_0} & \boldsymbol{u_1} & \cdots & \boldsymbol{u_{p-1}} & \cdots & \boldsymbol{u_{L-2}} \\ & \boldsymbol{y_0} & \boldsymbol{y_1} & \cdots & \boldsymbol{y_{p-1}} & \cdots & \boldsymbol{y_{L-2}} \\ & & \boldsymbol{u_0} & \cdots & \boldsymbol{u_{p-2}} & \cdots & \boldsymbol{u_{L-3}} \\ & & \boldsymbol{y_0} & \cdots & \boldsymbol{y_{p-2}} & \cdots & \boldsymbol{u_{L-3}} \\ & & & \ddots & \vdots & \cdots & \vdots \\ & & & & \boldsymbol{u_0} & \cdots & \boldsymbol{u_{L-p-1}} \\ & & & & \boldsymbol{y_0} & \cdots & \boldsymbol{y_{L-p-1}} \end{bmatrix} . \tag{4}$$

Throughout this report, the dimensions of the matrices and vectors are noted in blue below key equations. The order of the ARX model, *p*, and the number of samples, *L*, are specified by the user. Some guidelines for their selection are given in Juang (*6*). The matrix $\bar{Y}$, containing the OMPs, α_i and β_i, follows from equation 2 by inversion and has the following form:

$$\underset{\boldsymbol{m}\ \mathbf{x}\ [\boldsymbol{r_c} + (\boldsymbol{r_c} + \boldsymbol{m})\boldsymbol{p}]}{\bar{\boldsymbol{Y}}} = [\boldsymbol{\beta_0} \quad \boldsymbol{\beta_1} \quad \boldsymbol{\alpha_1} \quad \boldsymbol{\beta_2} \quad \boldsymbol{\alpha_2} \quad \ldots \quad \boldsymbol{\beta_p} \quad \boldsymbol{\alpha_p}] \ . \tag{5}$$

The one-step-ahead output prediction equation given by equation 1 is the starting point for deriving the multistep output prediction equation that is needed for deriving the GPC controller. This equation is obtained by replacing t by $t+j$ in equation 1, and letting j range over the set of values $j=1, 2, \ldots h_p\text{-}1$, where h_p is the prediction horizon (the number of time steps for which the future responses are predicted). The resulting equations can be assembled into a multistep output prediction equation having the following form:

$$\{\boldsymbol{y}_{\boldsymbol{h_p}}\} = \boldsymbol{\tau}\{\boldsymbol{u}_{\boldsymbol{h_c}}\} + \boldsymbol{\alpha}\{\boldsymbol{y}_{\boldsymbol{p}}\} + \boldsymbol{\beta}\{\boldsymbol{u}_{\boldsymbol{p}}\}\,. \tag{6}$$

The coefficient matrices τ, β, and α are formed from combinations of the OMP. The quantity y_{h_p} is the vector containing the future predicted responses, whereas u_{h_c} is the vector containing the (unknown) future control commands. The integer h_c is the control horizon (the number of time steps over which future control is assumed to act). The quantities u_p and y_p are vectors containing the previous p sets of control commands, and measured responses, respectively.

$$\begin{Bmatrix} y_{t+0} \\ \vdots \\ y_{t+h_p-1} \end{Bmatrix} = \begin{bmatrix} \beta_0 & & & \\ \beta_0^1 & \beta_0 & & \\ \vdots & \vdots & \ddots & \\ \beta_0^{q-1} & \beta_0^{q-2} & \cdots & \beta_0 \\ \beta_0^{q} & \beta_0^{q-1} & \cdots & \\ \vdots & \vdots & \cdots & \\ \beta_0^{h_p-1} & \beta_0^{h_p-2} & \cdots & \beta_0^{h_p-h_c} \end{bmatrix} \begin{Bmatrix} u_{t+0} \\ \vdots \\ u_{t+h_c-1} \end{Bmatrix}$$

mh_p x 1 $\qquad$ mh_p x $r_c h_c$ $\qquad$ $r_c h_c$ x 1

$$+ \begin{bmatrix} \alpha_1 & \alpha_2 & \cdots & \alpha_p \\ \alpha_1^1 & \alpha_2^1 & \cdots & \alpha_p^1 \\ \vdots & \vdots & \cdots & \vdots \\ \alpha_1^{q-1} & \alpha_2^{q-1} & \cdots & \alpha_p^{q-1} \\ \alpha_1^{q} & \alpha_2^{q} & \cdots & \alpha_p^{q} \\ \vdots & \vdots & \cdots & \vdots \\ \alpha_1^{h_p-1} & \alpha_2^{h_p-1} & \cdots & \alpha_p^{h_p-1} \end{bmatrix} \begin{Bmatrix} y_{t-1} \\ \vdots \\ y_{t-p} \end{Bmatrix}$$

mh_p x mp $\qquad$ mp x 1

$$+ \begin{bmatrix} \beta_1 & \beta_2 & \cdots & \beta_p \\ \beta_1^1 & \beta_2^1 & \cdots & \beta_p^1 \\ \vdots & \vdots & \cdots & \vdots \\ \beta_1^{q-1} & \beta_2^{q-1} & \cdots & \beta_p^{q-1} \\ \beta_1^{q} & \beta_2^{q} & \cdots & \beta_p^{q} \\ \vdots & \vdots & \cdots & \vdots \\ \beta_1^{h_p-1} & \beta_2^{h_p-1} & \cdots & \beta_p^{h_p-1} \end{bmatrix} \begin{Bmatrix} u_{t-1} \\ \vdots \\ u_{t-p} \end{Bmatrix}, \tag{7}$$

mh_p x $r_c p$ $\qquad$ $r_c p$ x 1

where the coefficients are calculated using the following relations:

$$\beta_0^q = \beta_1^{q-1} + \alpha_1^{q-1}\beta_0 \,. \tag{8}$$

$$\alpha_{p-1}^q = \alpha_p^{q-1} + \alpha_1^{q-1}\alpha_{p-1} \,. \tag{9}$$

$$\beta_{p-1}^q = \beta_p^{q-1} + \alpha_1^{q-1}\beta_{p-1} \,. \tag{10}$$

In this formulation the size of the ARX model, *p*, is set equal to the number of future predicted responses, h_p, (prediction horizon) and future commands, h_c, (control horizon). Generally, these three parameters can differ from one another (*1*, *2*).

The optimal control law is obtained by minimizing an objective function. To accomplish this, one defines a quadratic objective function as follows:

$$\boldsymbol{J} = \boldsymbol{y}_{\boldsymbol{h_p}}^{\boldsymbol{T}}\boldsymbol{Q}\boldsymbol{y}_{\boldsymbol{h_p}} + \boldsymbol{u}_{\boldsymbol{h_c}}^{\boldsymbol{T}}\boldsymbol{R}\boldsymbol{u}_{\boldsymbol{h_c}} \,, \tag{11}$$

where *Q* is a symmetric positive semi-definite matrix that assigns weights to the predicted responses, *R* is a symmetric positive definite matrix that assigns weights on the future control commands, and the superscript *T* indicates the vector or matrix transpose.

Substituting the expanded equation for *y* yields

$$\boldsymbol{J} = \left[\boldsymbol{\tau}\{\boldsymbol{u}_{\boldsymbol{h_c}}\} + \boldsymbol{\alpha}\{\boldsymbol{y}_{\boldsymbol{p}}\} + \boldsymbol{\beta}\{\boldsymbol{u}_{\boldsymbol{p}}\}\right]^{\boldsymbol{T}}\boldsymbol{Q}\left[\boldsymbol{\tau}\{\boldsymbol{u}_{\boldsymbol{h_c}}\} + \boldsymbol{\alpha}\{\boldsymbol{y}_{\boldsymbol{p}}\} + \boldsymbol{\beta}\{\boldsymbol{u}_{\boldsymbol{p}}\}\right] + \boldsymbol{u}_{\boldsymbol{h_c}}^{\boldsymbol{T}}\boldsymbol{R}\boldsymbol{u}_{\boldsymbol{h_c}} \,. \tag{12}$$

The minimum is obtained by taking the partial derivative of the function with respect to future commands,$\{u_{h_c}\}$, and setting it equal to zero.

$$\boldsymbol{0} = \frac{\boldsymbol{\partial}}{\boldsymbol{\partial u_{h_c}}}\left[\boldsymbol{\tau}\{\boldsymbol{u}_{\boldsymbol{h_c}}\} + \boldsymbol{\alpha}\{\boldsymbol{y}_{\boldsymbol{p}}\} + \boldsymbol{\beta}\{\boldsymbol{u}_{\boldsymbol{p}}\}\right]^{\boldsymbol{T}}\boldsymbol{Q}\left[\boldsymbol{\tau}\{\boldsymbol{u}_{\boldsymbol{h_c}}\} + \boldsymbol{\alpha}\{\boldsymbol{y}_{\boldsymbol{p}}\} + \boldsymbol{\beta}\{\boldsymbol{u}_{\boldsymbol{p}}\}\right] + \frac{\boldsymbol{\partial}}{\boldsymbol{\partial u_{h_c}}}\boldsymbol{u}_{\boldsymbol{h_c}}^{\boldsymbol{T}}\boldsymbol{R}\boldsymbol{u}_{\boldsymbol{h_c}} \,. \tag{13}$$

$$\boldsymbol{0} = \boldsymbol{2\tau}^{\boldsymbol{T}}\boldsymbol{Q}\left[\boldsymbol{\tau}\{\boldsymbol{u}_{\boldsymbol{h_c}}\} + \boldsymbol{\alpha}\{\boldsymbol{y}_{\boldsymbol{p}}\} + \boldsymbol{\beta}\{\boldsymbol{u}_{\boldsymbol{p}}\}\right] + \boldsymbol{2R}\begin{Bmatrix}\boldsymbol{u}_{\boldsymbol{t+0}}\\ \vdots \\ \boldsymbol{u}_{\boldsymbol{t+h_c}}\end{Bmatrix}. \tag{14}$$

Solving for control commands yields the following optimal future commands:

$$\{\boldsymbol{u}_{\boldsymbol{h_c}}\} = -(\boldsymbol{\tau}^{\boldsymbol{T}}\boldsymbol{Q}\boldsymbol{\tau} + \mathbf{R})^{-\mathbf{1}}\boldsymbol{\tau}^{\boldsymbol{T}}\boldsymbol{Q}\left[\boldsymbol{\alpha}\{\boldsymbol{y}_{\boldsymbol{p}}\} + \boldsymbol{\beta}\{\boldsymbol{u}_{\boldsymbol{p}}\}\right] \,. \tag{15}$$

Defining the following control law matrices,

$$\mathbf{A}_{\boldsymbol{C}} = -(\boldsymbol{\tau}^{\boldsymbol{T}}\boldsymbol{Q}\boldsymbol{\tau} + \mathbf{R})^{-\mathbf{1}}\boldsymbol{\tau}^{\boldsymbol{T}}\boldsymbol{Q}\boldsymbol{\alpha} \tag{16}$$

and

$$\mathbf{B}_{\boldsymbol{C}} = -(\boldsymbol{\tau}^{\boldsymbol{T}}\boldsymbol{Q}\boldsymbol{\tau} + \mathbf{R})^{-\mathbf{1}}\boldsymbol{\tau}^{\boldsymbol{T}}\boldsymbol{Q}\boldsymbol{\beta} \,, \tag{17}$$

yields control laws that calculate the next h_c sets of commands:

$$\{\boldsymbol{u}_{\boldsymbol{h_c}}\} = \mathbf{A_C}\{\boldsymbol{y}_{\boldsymbol{p}}\} + \mathbf{B_C}\{\boldsymbol{u}_{\boldsymbol{p}}\} \,, \tag{18}$$

where u_{h_c} corresponds to the control commands h_c time steps into the future.

However, only the first set of control commands will be applied to the system, thus only the first r_c rows of $\{u_{h_c}\}$ are needed. The remaining rows are discarded.

$$\underset{r_c \text{ x } 1}{\{\boldsymbol{u_{t+0}}\}} = \underset{r_c \text{ x } mp}{\boldsymbol{\alpha_C}} \underset{mp \text{ x } 1}{\begin{Bmatrix} \boldsymbol{y_{t-1}} \\ \vdots \\ \boldsymbol{y_{t-p}} \end{Bmatrix}} + \underset{r_c \text{ x } r_c p}{\boldsymbol{\beta_C}} \underset{r_c p \text{ x } 1}{\begin{Bmatrix} \boldsymbol{u_{t-1}} \\ \vdots \\ \boldsymbol{u_{t-p}} \end{Bmatrix}} . \tag{19}$$

4.2 GPC With Explicit Disturbance

Generalized Predictive Controller With Explicit Disturbance, as discussed in Juang and Eure (*1*) and Kvaternik et al. (*4*), is similar to GPC With Implicit Disturbance, except that now the external disturbances are explicitly measured and included in the model. Time histories of control commands, measurement responses, and now disturbance measurements are used to generate the ARX model for the system. The *V* matrix with disturbance information is shown next.

$$V = \underset{[r_d + r_c + (r_d + r_c + m)p] \text{ x } L}{\begin{bmatrix} d_0 & d_1 & \cdots & d_p & \cdots & d_{L-1} \\ u_0 & u_1 & \cdots & u_p & \cdots & u_{L-1} \\ & d_0 & \cdots & d_{p-1} & \cdots & d_{L-2} \\ & u_0 & \cdots & u_{p-1} & \cdots & u_{L-2} \\ & y_0 & \cdots & y_{p-1} & \cdots & y_{L-2} \\ & & \ddots & \vdots & \cdots & \vdots \\ & & & u_0 & \cdots & u_{L-p-1} \\ & & & y_0 & \cdots & y_{L-p-1} \end{bmatrix}} . \tag{20}$$

The new matrix $\bar{Y}$, containing the OMP, has the following form:

$$\underset{\boldsymbol{m} \text{ x } [\boldsymbol{r_d} + \boldsymbol{r_c} + (\boldsymbol{r_d} + \boldsymbol{r_c} + \boldsymbol{m})\boldsymbol{p}]}{\bar{\boldsymbol{Y}} = [\boldsymbol{\delta_0} \quad \boldsymbol{\beta_0} \quad \boldsymbol{\delta_1} \quad \boldsymbol{\beta_1} \quad \boldsymbol{\alpha_1} \quad \boldsymbol{\delta_2} \quad \boldsymbol{\beta_2} \quad \boldsymbol{\alpha_2} \quad \ldots \quad \boldsymbol{\delta_p} \quad \boldsymbol{\beta_p} \quad \boldsymbol{\alpha_p}]} . \tag{21}$$

These OMP values are used to predict future responses based on past responses (including external disturbances) and control commands.

$$\{\boldsymbol{y_{h_p}}\} = \boldsymbol{\tau}\{\boldsymbol{u_{h_c}}\} + \boldsymbol{\alpha}\{\boldsymbol{y_p}\} + \boldsymbol{\beta}\{\boldsymbol{u_p}\} + \boldsymbol{\delta}\{\boldsymbol{d_p}\} . \tag{22}$$

$$\begin{Bmatrix} \boldsymbol{y_{t+0}} \\ \vdots \\ \boldsymbol{y_{t+h_p}} \end{Bmatrix} = \boldsymbol{\tau} \begin{Bmatrix} \boldsymbol{u_{t+0}} \\ \vdots \\ \boldsymbol{u_{t+h_c}} \end{Bmatrix} + \boldsymbol{\alpha} \begin{Bmatrix} \boldsymbol{y_{t-1}} \\ \vdots \\ \boldsymbol{y_{t-p}} \end{Bmatrix} + \boldsymbol{\beta} \begin{Bmatrix} \boldsymbol{u_{t-1}} \\ \vdots \\ \boldsymbol{u_{t-p}} \end{Bmatrix} + \boldsymbol{\delta} \begin{Bmatrix} \boldsymbol{d_{t-1}} \\ \vdots \\ \boldsymbol{d_{t-p}} \end{Bmatrix} . \tag{23}$$

As before, the next control commands are calculated by minimizing the objective function and taking the partial derivative with respect to control commands; the rows corresponding to future control commands are dropped. Using this extension, we can use the measured disturbance information.

$$\{\boldsymbol{u}_{t+0}\} = \boldsymbol{\alpha}_C \begin{Bmatrix} \boldsymbol{y}_{t-1} \\ \vdots \\ \boldsymbol{y}_{t-p} \end{Bmatrix} + \boldsymbol{\beta}_C \begin{Bmatrix} \boldsymbol{u}_{t-1} \\ \vdots \\ \boldsymbol{u}_{t-p} \end{Bmatrix} + \boldsymbol{\delta}_C \begin{Bmatrix} \boldsymbol{d}_{t-1} \\ \vdots \\ \boldsymbol{d}_{t-p} \end{Bmatrix} \quad . \tag{24}$$

r_c x 1 ; mp x 1 ; $r_c p$ x 1 ; $r_d p$ x 1

r_c x mp ; r_c x $r_c p$; r_c x $r_d p$

4.3 GPC With Preview Control

Preview Control or Look-Ahead Control measures the external disturbance before it affects the vehicle and incorporates this information into the control algorithms. Preview Control was first published in Bender (*7*) and is further developed in Van der Aa (*8*) and El Madany et al. (*9*) for linear full-state feedback control.

Generalized Predictive Controller With Preview Control is a direct extension of GPC With Explicit Disturbance. If it is possible to generate a model of the explicit disturbance to predict future disturbances (*4*), then this future information can be used in conjunction with the control command, external disturbance, and measured response time histories to generate the future control commands. This research, however, assumes that the future disturbance can be directly measured using vehicle-based sensors. Again, time histories of controls commands, measurement responses, and disturbance measurements are used to generate the ARX model for the system. The matrix $\bar{Y}$ is identical to equation 21.

These time histories are used to predict future responses based on past responses, past and future disturbances, and past and future control commands. In this formulation, we assume that the current and future disturbance can be measured. The matrix γ is the component of the ARX model that corresponds to the current and future disturbances.

$$\begin{Bmatrix} \boldsymbol{y}_{t+0} \\ \vdots \\ \boldsymbol{y}_{t+h_p} \end{Bmatrix} = \boldsymbol{\tau} \begin{Bmatrix} \boldsymbol{u}_{t+0} \\ \vdots \\ \boldsymbol{u}_{t+h_c} \end{Bmatrix} + \boldsymbol{\gamma} \begin{Bmatrix} \boldsymbol{d}_{t+0} \\ \vdots \\ \boldsymbol{d}_{t+h_c} \end{Bmatrix} + \boldsymbol{\alpha} \begin{Bmatrix} \boldsymbol{y}_{t-1} \\ \vdots \\ \boldsymbol{y}_{t-p} \end{Bmatrix} + \boldsymbol{\beta} \begin{Bmatrix} \boldsymbol{u}_{t-1} \\ \vdots \\ \boldsymbol{u}_{t-p} \end{Bmatrix} + \boldsymbol{\delta} \begin{Bmatrix} \boldsymbol{d}_{t-1} \\ \vdots \\ \boldsymbol{d}_{t-p} \end{Bmatrix} . \tag{25}$$

As before, the future control commands are calculated by minimizing the objective function and taking the partial derivative with respect to control commands; only the rows corresponding to the next immediate control commands are retained. Using this extension, we can use both the future and the previous measured disturbance information.

$$\{\boldsymbol{u}_{t+0}\} = \boldsymbol{\gamma}_C \begin{Bmatrix} \boldsymbol{d}_{t+0} \\ \vdots \\ \boldsymbol{d}_{t+h_c} \end{Bmatrix} + \boldsymbol{\alpha}_C \begin{Bmatrix} \boldsymbol{y}_{t-1} \\ \vdots \\ \boldsymbol{y}_{t-p} \end{Bmatrix} + \boldsymbol{\beta}_C \begin{Bmatrix} \boldsymbol{u}_{t-1} \\ \vdots \\ \boldsymbol{u}_{t-p} \end{Bmatrix} + \boldsymbol{\delta}_C \begin{Bmatrix} \boldsymbol{d}_{t-1} \\ \vdots \\ \boldsymbol{d}_{t-p} \end{Bmatrix} . \tag{26}$$

The difference in control command between GPC With Explicit Disturbance and GPC With Preview Control is solely due to the presence of the future disturbance term. The control matrices, α_C, β_C, and δ_C are the same for both control laws.

5. Road Profiles

Three road profiles were used to evaluate the algorithms: Sine, Curb, and Perryman3. In each case, the road profiles were provided as an array of ground distances and vertical heights.

5.1 Sine Road Profile

This road profile was defined by a sine wave with a half-amplitude of 0.10 m and a wavelength of 10 m. The intent was to provide a single-frequency disturbance that relates to vehicle speed—in this case, 1 m/s (3.6 km/h) of speed corresponds to 0.1 Hz excitation. There is a 30-m flat stretch to allow the model to reach steady state after startup. Figure 3 shows a portion of this type of road profile.

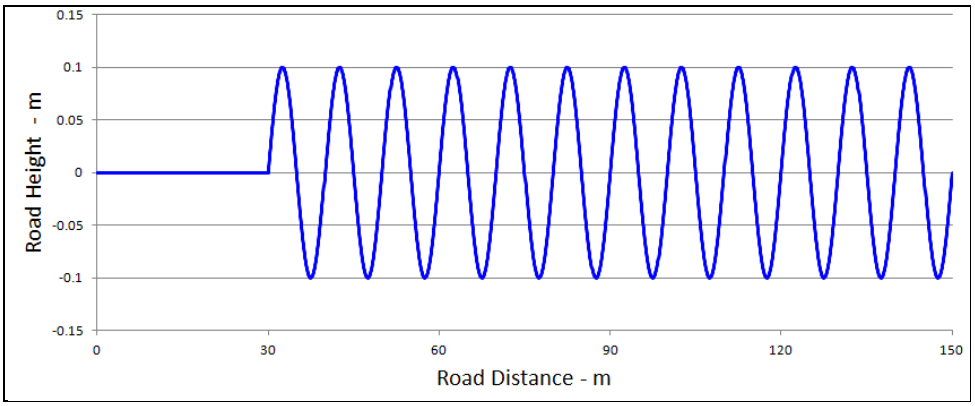

Figure 3. Sine road profile.

5.2 Curb Road Profile

This road profile is defined by a 0.10-m step rise followed by 10 m of level surface, and then a 0.10-m step drop, as shown in figure 4. The intent was to provide a step input disturbance into the system. There is a 30-m flat stretch to let the initial oscillations die out and the vehicle reach steady state.

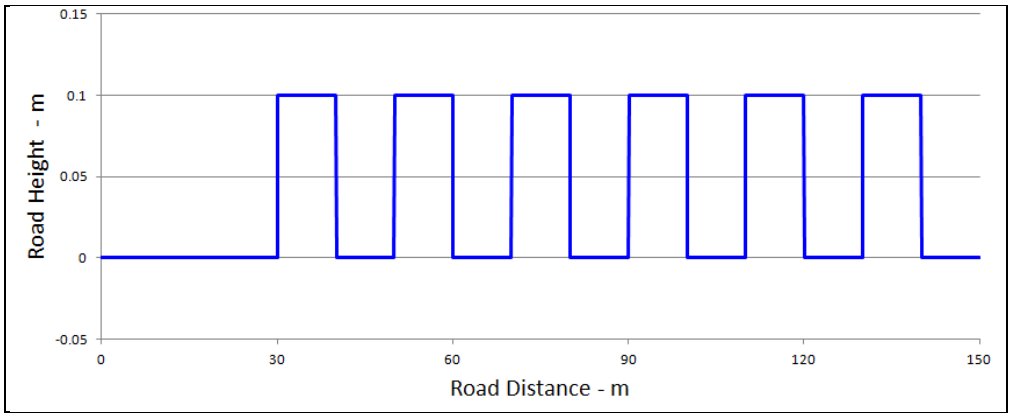

Figure 4. Curb road profile.

5.3 Perryman3 Road Profile

Perryman3 is an off-road test track located at the Aberdeen Proving Ground. This road profile, shown in figure 5, is intended to evaluate the algorithms against a challenging "real-world" course.

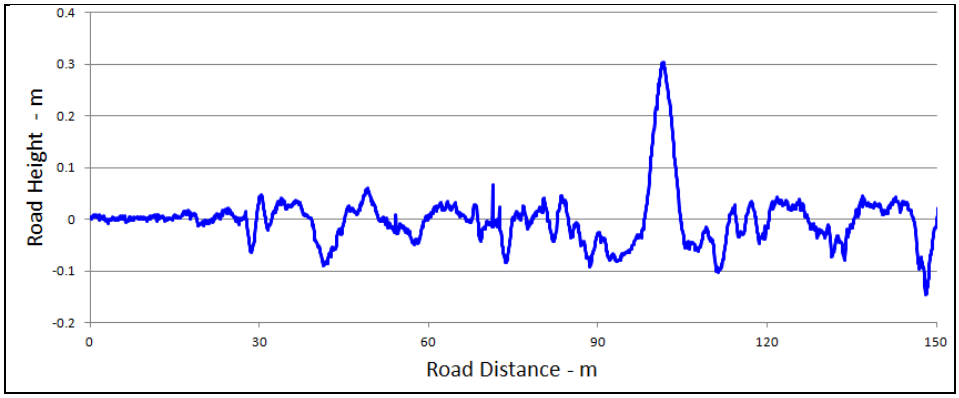

Figure 5. Perryman3 road profile.

6. Simulation Results: Linear GPC Variants

Simulations were run until the vehicle traveled 150 m. The open-loop model was run in parallel with closed-loop GPC With Implicit Disturbance, GPC With Explicit Disturbance, and GPC With Preview Control for performance comparison studies. All measurements assumed no noise or offset bias. Initial conditions for the suspension system state variables were set to zero. Vehicle speed was held at a constant value for the entire run.

For this work the system identification for each algorithm was precomputed. Band-limited white noise was used to excite the four actuators. The vehicle was run over the Perryman3 terrain profile at 40 km/h. This provided broadband random disturbance inputs out to 50 Hz with large peaks from 0.5 to 3 Hz.

The following objective functions were used as metrics in several comparisons of algorithm performance:

$$\boldsymbol{J_{Resp} = \ low\ pass}(\sqrt{\boldsymbol{y^T y}}\,)\ , \tag{27}$$

$$\boldsymbol{Actuator\ Force = \ low\ pass}(\sqrt{\boldsymbol{u^T u}}\,)\ , \tag{28}$$

and

$$\boldsymbol{Actuator\ Power = \ low\ pass}(\sqrt{(\boldsymbol{power^T power}}\,)\ , \tag{29}$$

where "low pass" denotes a fourth-order digital low-pass Butterworth filter with a cutoff frequency of 1 Hz.

Using the cosine double angle formula, we see that the square of a signal will have a steady offset component and a high-frequency component that is twice the frequency of the original signal. The low-pass filter removes the oscillatory component, leaving only the steady offset, which is related to the amplitude of the fast Fourier transform of the original signal. Because the cutoff frequency is higher than the lowest frequency of excitation in the road profiles, there is a small low-frequency oscillation in the objective function, *J*. The low-frequency oscillation is removed by averaging the objective function over the entire run time.

For each simulation, the averaged values of *J* were plotted for a series of vehicle speeds up to 80 km/h. The closed-loop responses were normalized by the corresponding values of the open-loop responses at each speed.

$$\boldsymbol{Response\ Improvement} = \mathbf{1} - \frac{\boldsymbol{J_{Resp,algorithm}}}{\boldsymbol{J_{Resp,open\ loop}}}\ . \tag{30}$$

This normalization allows a more meaningful comparison of the algorithms despite the variation in actuator force or power.

$$\begin{matrix}\boldsymbol{Force\ Normalized} \\ \boldsymbol{Effectiveness}\end{matrix} = \frac{\boldsymbol{Response\ Improvement_{algorithm}}}{\boldsymbol{Actuator\ Force_{algorithm}}}\ . \tag{31}$$

$$\begin{matrix}\boldsymbol{Power\ Normalized} \\ \boldsymbol{Effectiveness}\end{matrix} = \frac{\boldsymbol{Response\ Improvement_{algorithm}}}{\boldsymbol{Actuator\ Power_{algorithm}}}\ . \tag{32}$$

Simulation results based on the modified HMMWV parameters are presented in figures 6–12. These figures were generated using the following algorithm parameters, as shown in table 2.

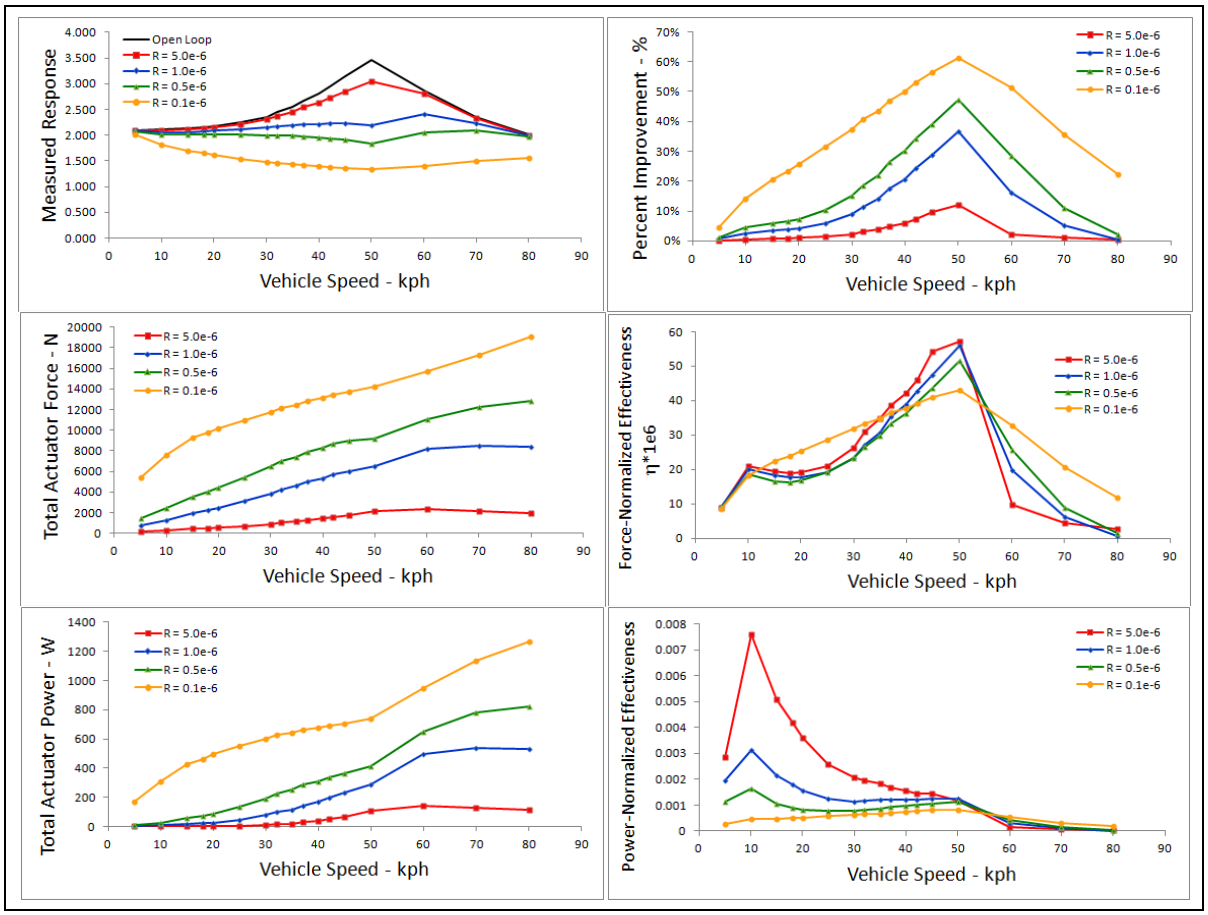

Figure 6. Effect of control weights on GPC with preview control on Sine road profile.

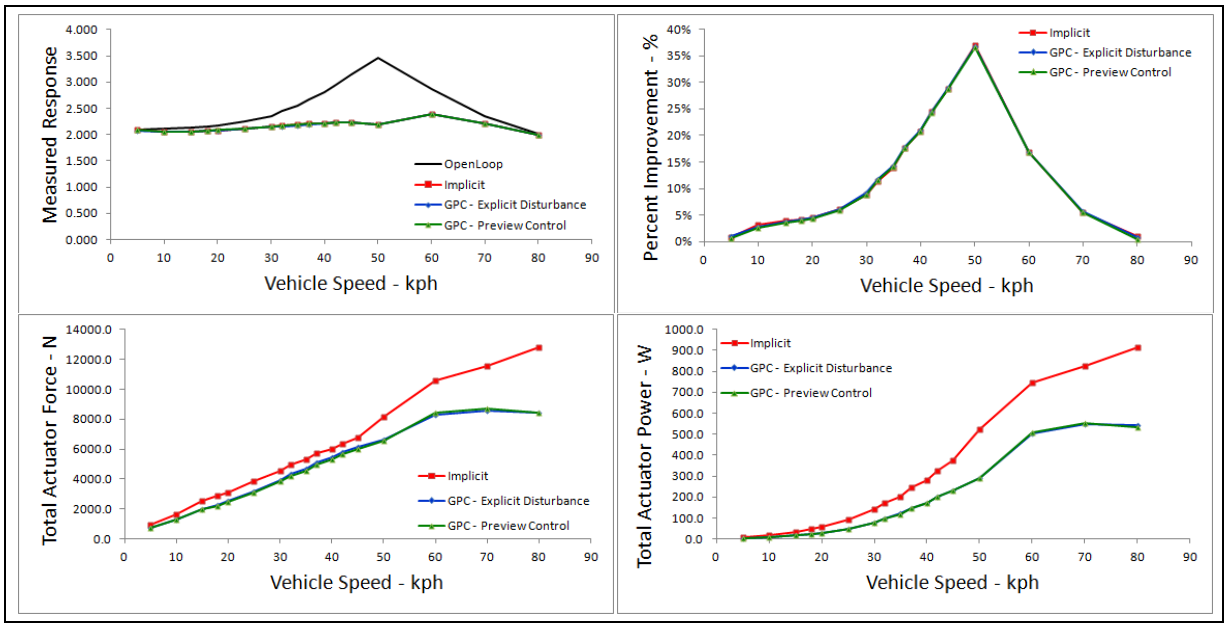

Figure 7. Effect of GPC algorithms on Sine road profile.

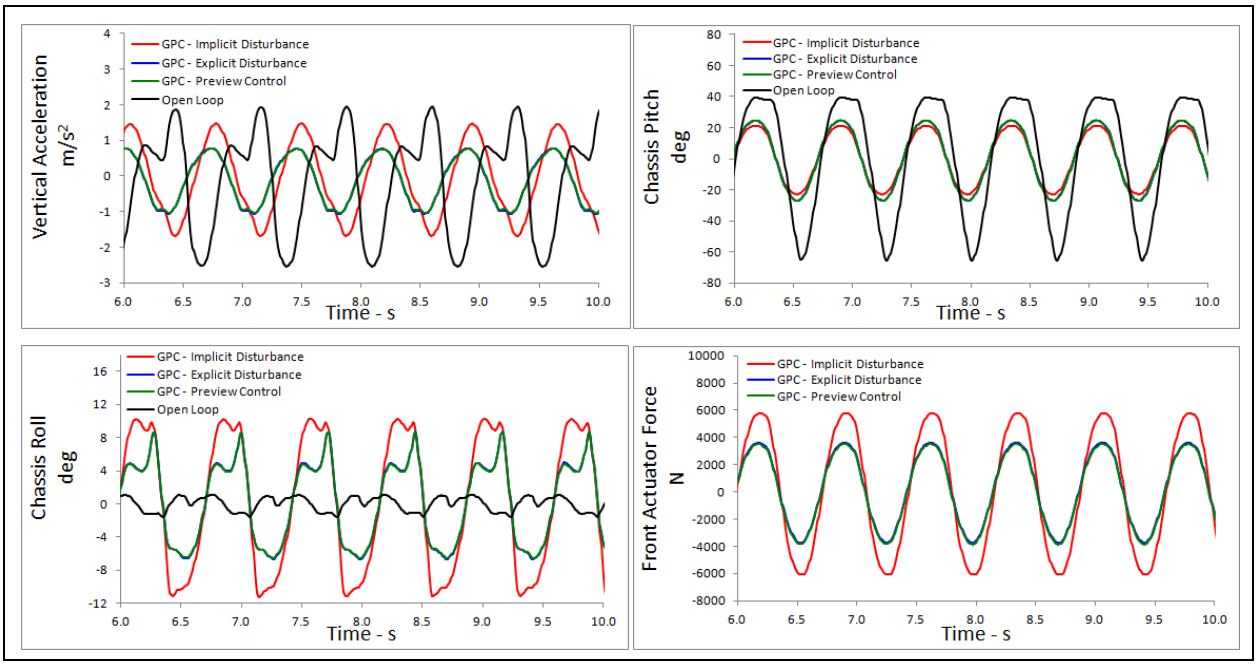

Figure 8. Time history of control algorithms for light vehicle parameters on Sine course at 50 km/h.

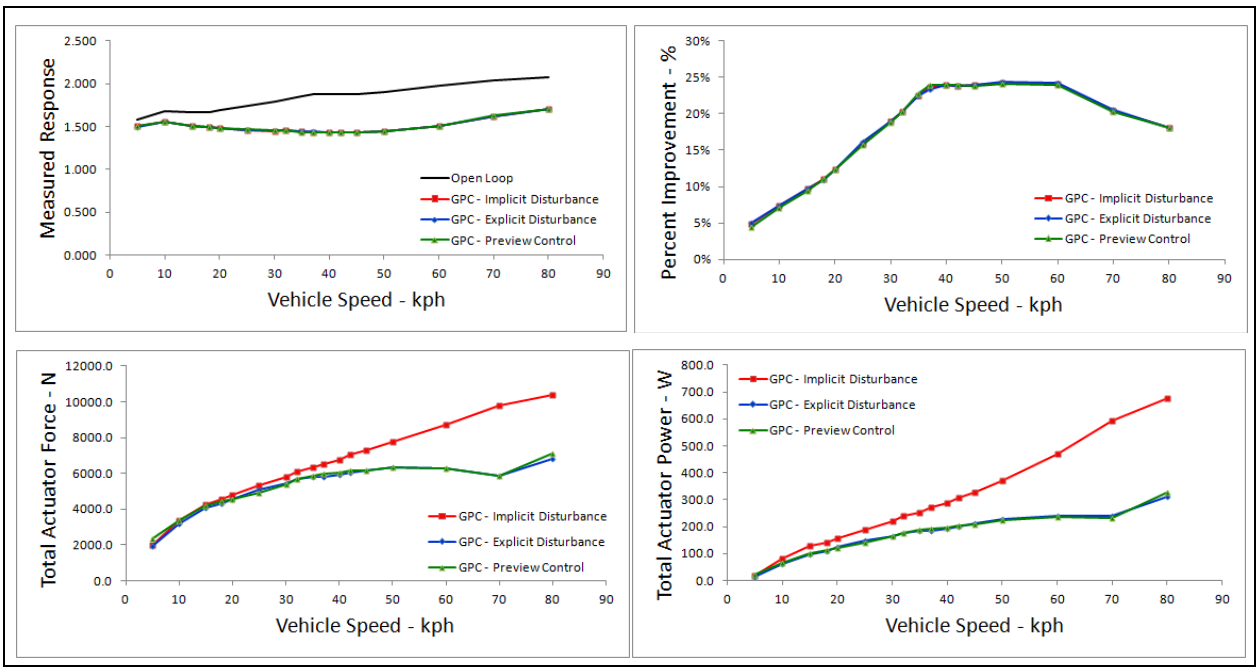

Figure 9. Effect of GPC algorithms for modified HMMWV on Perryman3 road profile.

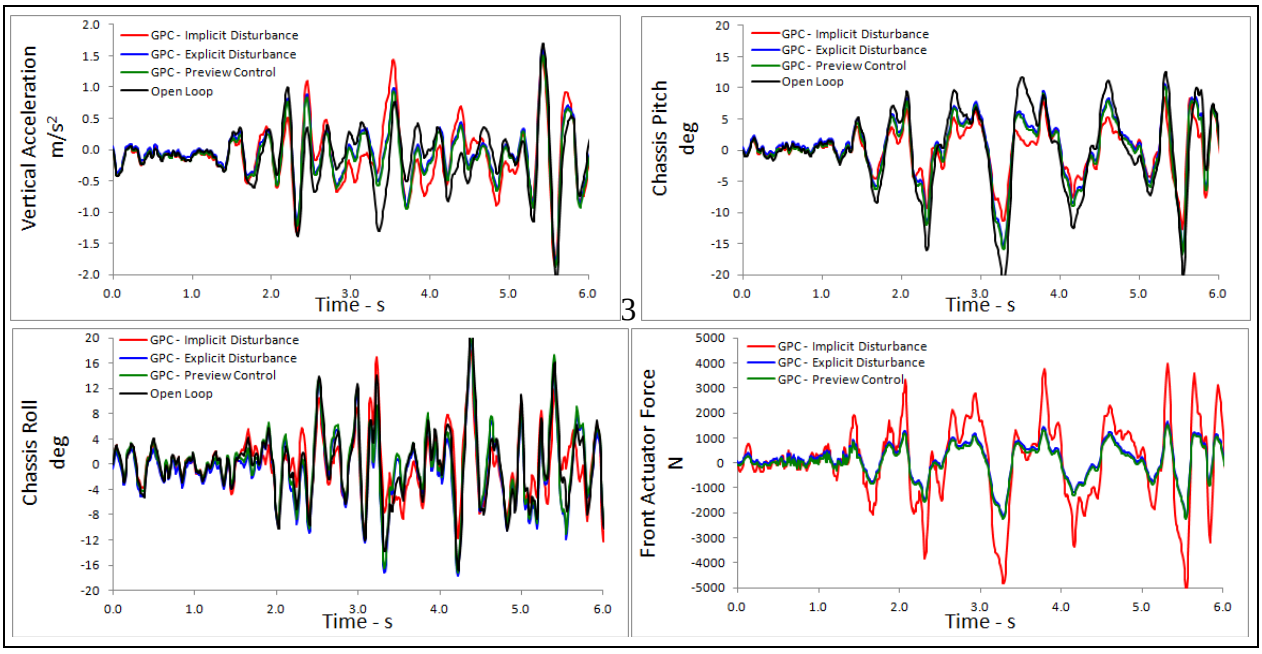

Figure 10. Time history of GPC algorithms for modified HMMWV parameters on Perryman3 course at 50 km/h.

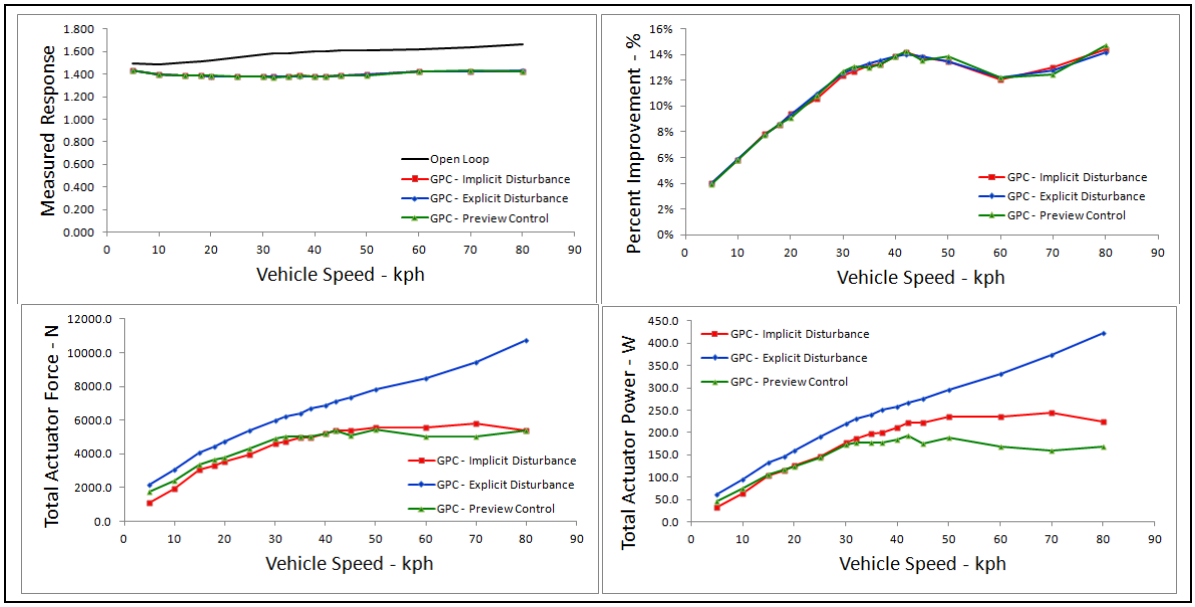

Figure 11. Effect of GPC algorithms on Curb road profile.

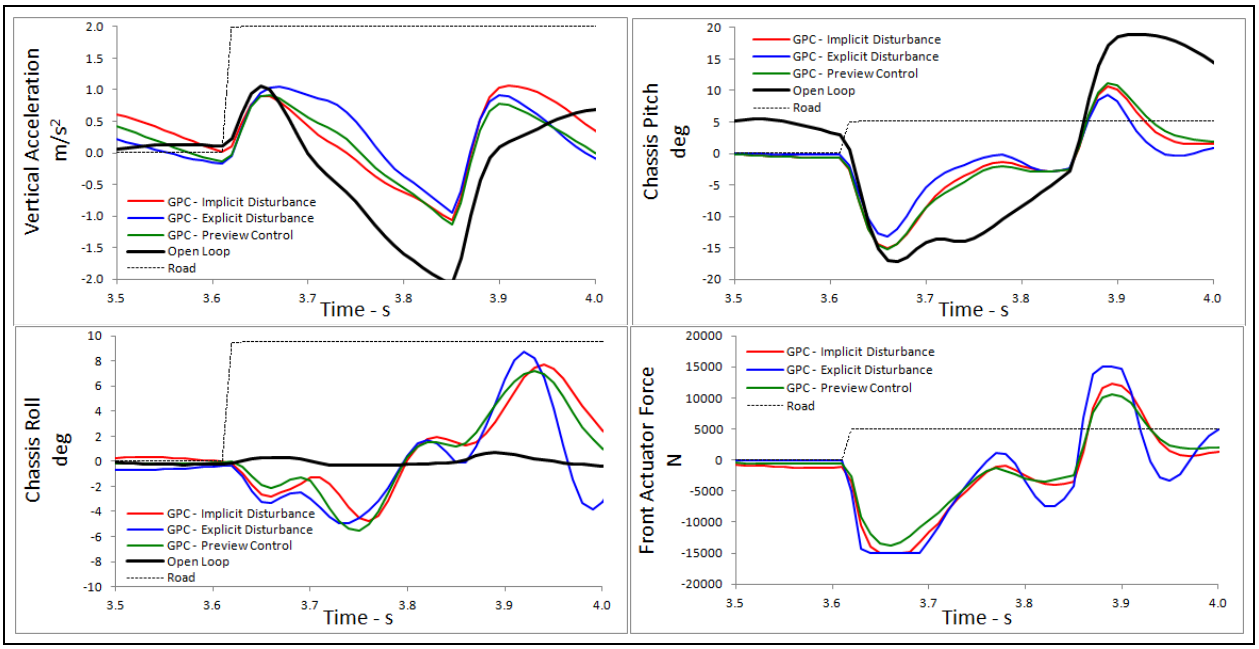

Figure 12. Time history of GPC algorithms for light vehicle parameters on Curb course at 72 km/h.

Table 2. Algorithm tuning parameters used for modified HMMWV vehicle.

Parameter	GPC With Implicit Disturbance	GPC With Explicit Disturbance	GPC With Preview Control
Actuators, r_c	4		
Disturbances, r_d	4		
Sensors, m	3		
Q	50 (vertical acceleration), 10 (pitch), 1 (roll)		
R	range { 1e-7 to 5e-6 }		
ARX model size, p	8		
Prediction horizon, h_p	8		
Control horizon, h_c	8		
Preview horizon	—	—	8 (0.08s)
ID sample size, L	400 points		
Disturbance for ID	Perryman 3 at 40 km/h		
Actuator ID signal	White noise		
Actuator limit	1.5e5 N		

6.1 Effects of Control Weighting

The modified HMMWV model was run with GPC With Preview Control over the Sine road profile from 0 to 80 km/h.

The objective function, actuator force, and actuator power are averaged over a 150-m simulation. The speed range corresponds to a sinusoidal excitation of 0 to 2.2 Hz. This is repeated several times for a range of control weights (R matrix values); the response weights (Q matrix values) were held constant. This effect of the control weighting matrix is shown in figure 6.

An order of magnitude decrease in the control weight matrix significantly improves the response and increases the required force and power. The force-normalized effectiveness shows that the curves for each weight coalesce in the same regions; the exception of R = 0.1e-6 occurs because the forces required are at the limit for the actuator. This suggests that as long as the commanded forces are within the capability of the actuator, the level of the response is linear with control loads. However, when comparing the actuator power, the power-normalized effectiveness decreases as the control weights decrease. This shows that the actuator power costs increase much faster than the responses decrease. Actuator power, then, becomes the driving factor for choosing control weights.

6.2 Comparison of Linear GPC Algorithms

A short comparison of the three control laws operating on the three road courses (disturbance inputs) is presented in the following discussion. The control weight for GPC With Explicit Disturbance was R = 1.0e-7 over the entire speed range. To simplify analysis, the control weights for the other two algorithms were chosen such that the magnitude of the measured responses matched GPC With Explicit Disturbance at each speed. Again, the objective function and the actuator force are averaged over the 150-m run for sinusoidal disturbances from 0 to 80 km/h (corresponding to 0 to 2.2 Hz). Figure 7 compares the three algorithms vs. vehicle speed.

The open-loop response reaches a peak at 50 km/h, representing the vehicle's pitch mode resonance frequency. The closed-loop algorithms reduce the peak by 60%, effectively attenuating the natural frequency. The normalized data shows that GPC With Explicit Disturbance and GPC With Preview Control have similar performance, requiring the same actuator force and power. However, GPC With Implicit requires significantly greater actuator force and power—almost twice the actuator power at 80 km/h. The addition of road disturbance information to the GPC algorithm greatly reduces the actuator loads for the closed-loop system.

Figure 8 is a time history of the measured responses and actuator forces for each algorithm as the vehicle maneuvers over the Sine road profile at 50 km/h, which represents a single-frequency disturbance of 1.4 Hz.

All three versions of the GPC algorithm reduce the chassis vertical acceleration and pitch. Chassis roll increases because of the very low response weight assigned to chassis roll. GPC With Implicit Disturbance performs worse on controlling chassis vertical acceleration but slightly better at reducing chassis pitch. Since the chassis pitch is the dominant term in the objective function, similar levels result for the response objective function. It is clear that GPC With Implicit Disturbance requires much higher actuator loads than the other two algorithms.

The same simulations were run using the Perryman3 road profile; the algorithm performance is shown in figure 9. The GPC algorithms reduce the overall response by more than 25% from the highest open-loop response. Much like the performance on the Sine road profile, GPC With Explicit Disturbance and GPC With Preview Control have almost identical response and actuator objective functions. Once again, GPC With Implicit Disturbance requires significantly higher actuator forces and loads to match the response objective function.

The GPC algorithms reduce the peaks of the chassis pitch compared to open-loop cases. This dominant sensor makes up for the slight increases in closed-loop roll and vertical acceleration. Without measured knowledge of the disturbance, GPC With Implicit Disturbance must wait until the sign of the responses changes before applying a countering force. This change results in the large, but brief, forces as the algorithm catches up to the changing slope of the disturbance. The algorithms with disturbance information have a much quicker response, thus reducing the peaks. The time history of the vehicle on Perryman3 is shown in figure 10.

The performance of the algorithms for the Curb road profile is shown in figure 11. Again, all three GPC algorithms reduce the response objective function by as much as 14% at the highest speed. However, this time there is a surprising difference between the actuator force and power of the algorithms. GPC With Explicit Disturbance requires the highest actuator loads, double the force and power as required for GPC With Implicit Disturbance. GPC With Preview Control requires the least power of the three variants—less than 200 W above 50 km/h, as shown in figure 11.

Previously, GPC With Explicit Disturbance was nearly indistinguishable from GPC With Preview Control. Figure 12 provides a closer look at the actuator forces experienced as the vehicle encounters the step height increase of the road. When the GPC With Explicit Disturbance encounters a step increase in the disturbance height (basically, a very steep slope), this steep slope produces a high control command. The steep slope is in the disturbance history for eight time steps.

On the other hand, GPC With Preview Control issues small commands (100 N) for the eight time steps prior to the start of the curb. This reduces the peak force required once the tire contacts the curb, resulting in the lowest peak force. Additionally, after the tire contacts the curb, the future disturbance contains eight time steps of flat data to further temper the control commands.

As before, GPC With Implicit Disturbance is unaware of the disturbance and can only respond after the measured responses are affected by the curb. Thus, it commands high peaks but not in response to an infinite slope.

7. Simulation With Nonlinear GPC

The research focus was to demonstrate nonlinear system identification and control of a quarter-car suspension system. The requirement for nonlinearity is driven by the use of semi-active MR dampers, which are inherently nonlinear. The algorithm that was considered and developed for this task is called bilinear generalized predictive control (bGPC). The bGPC algorithm is an extension of the previous work completed at ARL-VTD on GPC with an implicit disturbance model. The bGPC algorithm includes two additional terms in comparison to GPC—namely, future commands coupled with future responses and the past commands coupled with past responses. The NASA report by Jer-Nan Juang (*10*) describes the formulation of this type of model predictive control algorithm. The results of this system ID and controller (bGPC) were obtained using simulation with a quarter-car suspension model with MR damper. The vehicle parameters from a generic vehicle model from previously conducted research (*11*) at ARL-VTD were used in a quarter-car suspension model, as shown in figure 13. The predictions from dynamic simulations of the bGPC algorithm for a Sine wave road profile are shown in figure 14. The effects on chassis acceleration and percentage improvement between open-loop and bGPC closed-loop cases are shown in figure 14. Also, a full vehicle multibody dynamics model developed using TruckSim was used to analyze the effectiveness of the bGPC algorithm through cosimulation. Figure 15 shows the performance of the bGPC algorithm on a modified HMMWV model (TruckSim model) for the Perryman3 road profile. The simulation results (figure 15) show ~11% improvement for the most challenging Perryman3 terrain profile.

A different type of nonlinear control algorithm, called single experiment–multiple pulses, was also considered and developed using Matlab/Simulink. This algorithm uses a series of impulses to excite the command inputs and generate a system ID from those responses. For this algorithm development, a simplified linear quadratic regulator was used and adapted to implement closed-loop control. However, this control algorithm was unstable in system ID simulation and hence was dropped from the research effort.

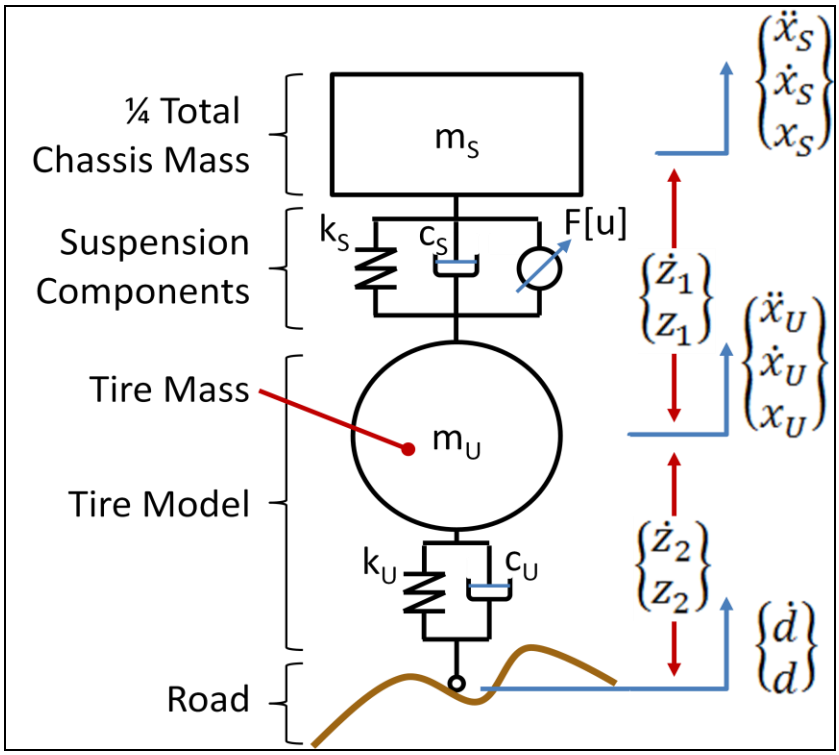

Figure 13. Quarter-car suspension model.

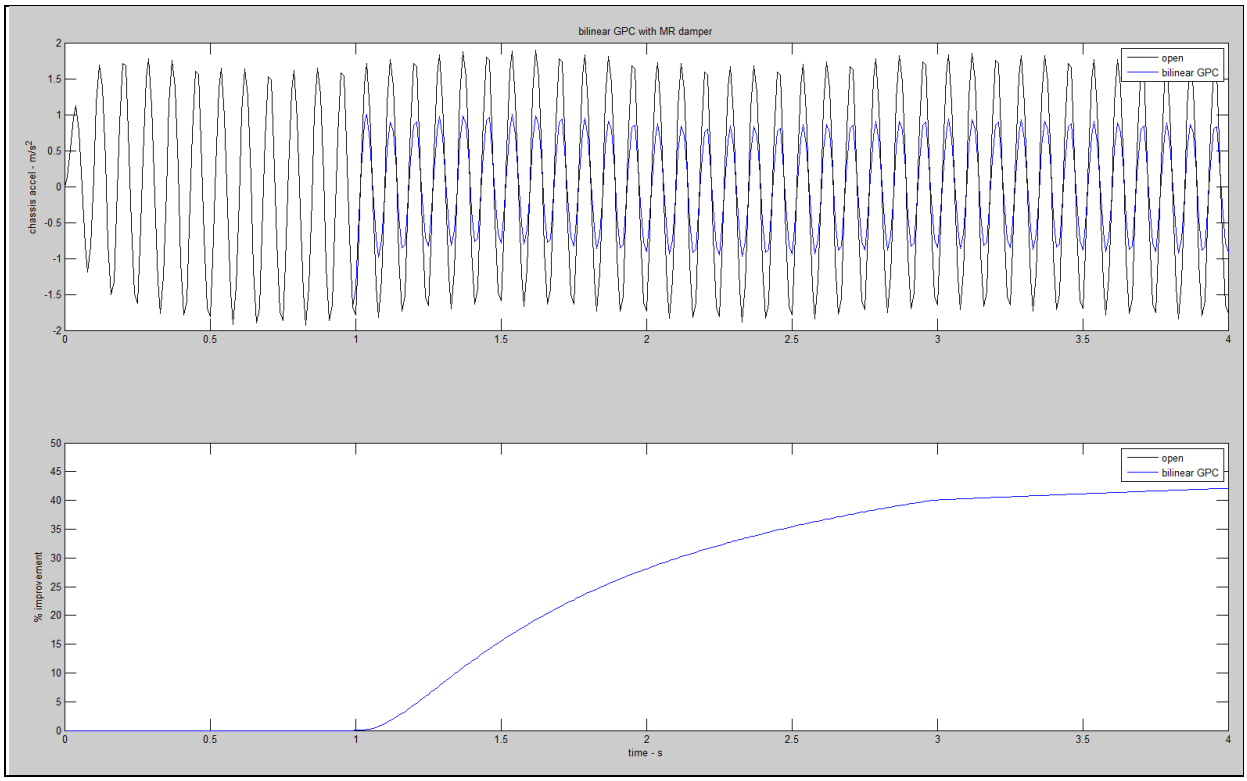

Figure 14. Comparison of bGPC algorithm with quarter-car model for Sine road profile.

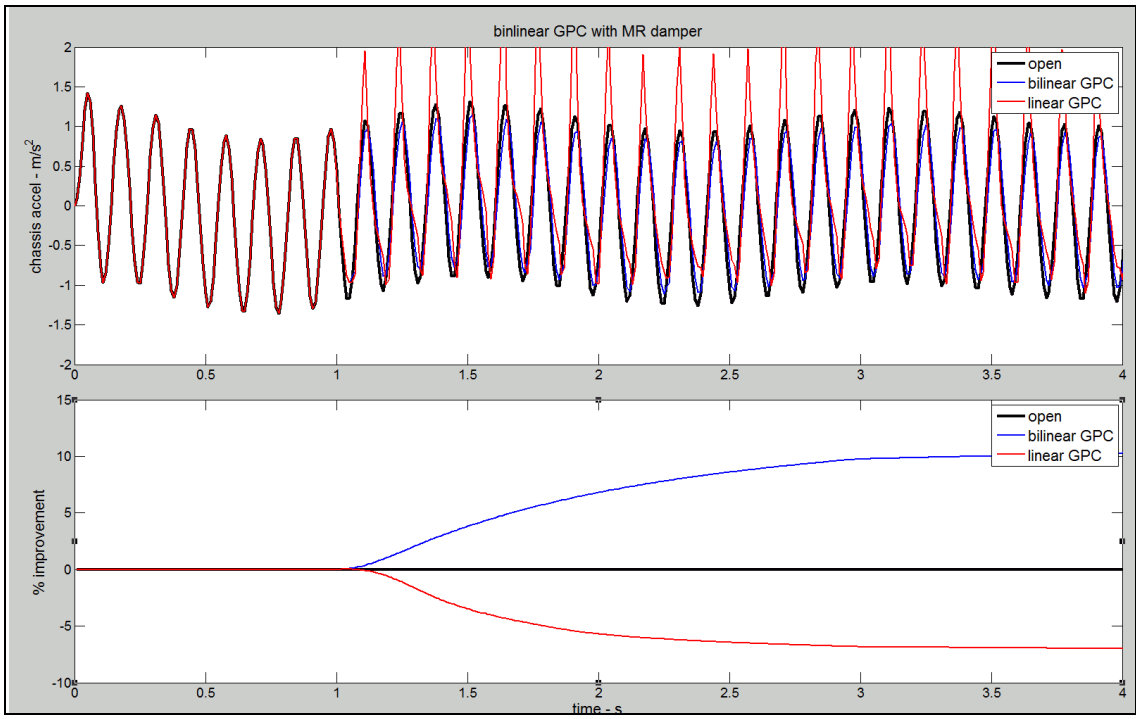

Figure 15. Performance of bGPC vs. linear GPC and open-loop cases (modified HMMWV model with Perryman3 profile).

8. Joint Research With University of Maryland on Advanced MR Damper

Semi-active shock and vibration isolation systems using MR energy absorbers (MREAs) require minimization of the field-off damping force at high speed (disabling additional stiffness generated by magneto-rheological fluid effects). This is because the viscous damping force for high shaft speed becomes excessive and will transmit the terrain-induced vibration to the vehicle body. This effect indicates that the controllable dynamic force range, defined as the ratio of the field-on damping force to the field-off damping force, is dramatically reduced. In addition, fail-safe MREA performance, if power were lost, is important to shock and vibration isolation systems. A key design goal is to minimize the field-off damping force while maximizing MREA dynamic force and also maintaining fail-safe performance. This ARL BAA research has come up with the principle of a bidirectional, controllable MREA that can produce large damping force and dynamic force range, as well as excellent fail-safe performance. The structural design of this device consists of electromagnetic coils and permanent magnets alternatively arranged in the inner cylinder of the device, as shown in figure 16. The permanent magnetic fields generated by the permanent magnets can be changed or even totally cancelled by applying negative current to the electromagnetic coils. A particular advantage of this magnetic circuit is that a fail-safe damping force in the event of lost power is provided by the permanent magnets. The damping

force of the MREA can be increased (or decreased) when applying positive (or negative) current to the electromagnetic coils to strengthen (or weaken) the magnetic field strength in the magnetic flux path, which realizes bidirectional control of the MREA damping force. The University of Maryland fabricated a baseline prototype of this MREA device. This MR damper will be used in the ASTR at ARL-VTD for carrying out verification and validation of developed control algorithms.

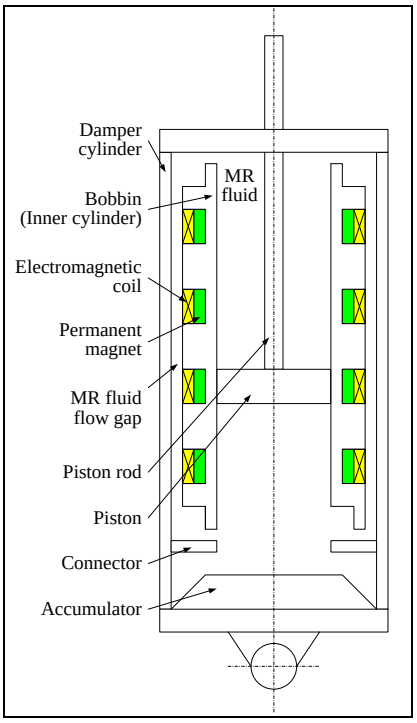

Figure 16. Bidirectional controllable inner bypass MR damper with fail-safe capability.

9. Advanced Suspension Test Rig (ASTR)

A 2-DOF ASTR has been fabricated to provide a basis for validating control laws that are developed. The test rig has variable sprung and unsprung masses of up to 250 kg, representing a 1000-kg ground vehicle. The tire and suspension components can be reconfigured using commercial off-the-shelf components or custom-made prototype components as needed. This test rig will be modified during FY 2013 to adapt it for use on the MTS load frame testing machine that ARL-VTD recently purchased. This load frame machine will be used to input road profile disturbances into the suspension system and study the effectiveness of control algorithms.

The suspension damper, shown in the figure 17, is replaceable with advanced active or semi-active dampers depending on our research interests. dSPACE hardware equipment has been purchased as well to conduct hardware-in-the-loop experiments for validating control laws. The control algorithm verification and validation tests are planned to be conducted during FY 2013.

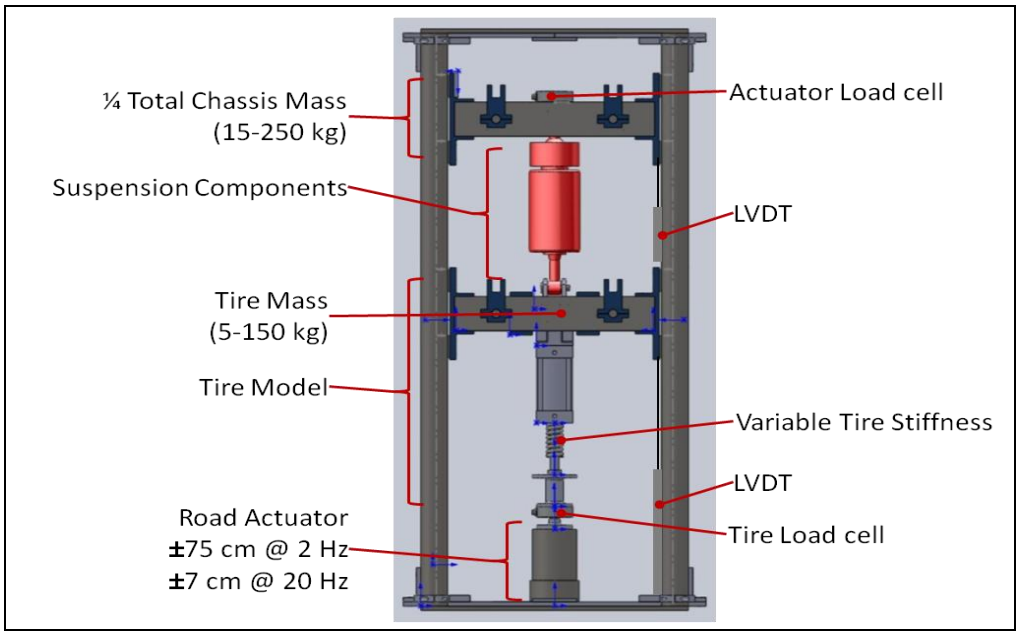

Figure 17. ASTR for quarter-car representation.

10. Conclusions

This section summarizes the results of numerical simulations directed at evaluating the effectiveness of GPC for the active control of chassis suspension systems in Army wheeled vehicles. GPC is a linear time-invariant, multi-input/multi-output predictive control method that uses an ARX model to describe the input-output relationship characterizing the system. The coefficient matrices of the ARX equation are determined using system identification techniques and are then used to form the matrices comprising the GPC control law. Key equations in the formulation of the method were summarized.

Three variants of the basic GPC linear algorithm were investigated. The first assumes that the disturbances are unknown and computes the control law, taking implicit account of the disturbances acting on the system (GPC With Implicit Disturbance). The second assumes that the past values of the disturbances can be measured and uses that information in deriving the control law (GPC With External Disturbance). The third variant assumes that the disturbances ahead of the vehicle can be measured and additionally uses that data when deriving the control

law (GPC With Preview Control). Closed-loop behavior of the system was simulated using a full-vehicle nonlinear model of a two-axle tactical vehicle moving over three types of road profile disturbances for each of the three GPC variants and compared to the open-loop behavior of the system. These comparisons show significant reductions in the chassis motions of the model.

Simulation has shown that for a given algorithm, the control weights reduce sensor objective function at the same rate that they increase actuator objective function. Thus, the control weight can be directly used to scale the total force available to a controller. GPC With Implicit Disturbance consistently requires higher actuator forces and more power than GPC With Preview Control or GPC With Explicit Disturbance when given a tonal or broadband disturbance. GPC With Preview Control performs nearly identically to baseline GPC With Explicit Disturbance; however, the preview control algorithm does drastically reduce the initial pulse due to step inputs. Despite the presence of disturbance information, GPC With Explicit Disturbance performs poorly on step road profile, even worse than having no disturbance information at all.

In summary, for the three road course profiles investigated, GPC With Preview Control performs better overall than the other GPC variants for reducing vehicle-chassis acceleration and pitch. The simulation results show that linear GPC With Preview Control is capable of reducing the vehicle-chassis acceleration by as much as 25% on average for the most challenging terrain profile course simulated with active suspension system. However, the nonlinear version—namely, bGPC—shows ~11% improvement for the most challenging Perryman3 terrain profile. The differences in the performance of the various algorithms studied in this research effort are currently being examined further to understand the main causes for the observed performance differences. In the future, these GPC algorithms will be tested using a 2-DOF suspension test rig at the Army Vehicle Research Laboratory to verify and validate these algorithms.

11. References

1. Juang, J.-N.; Eure, K. W. Predictive Feedback and Feedforward Control for Systems With Unknown Disturbances. Technical Memorandum 1998-208744; National Aeronautics and Space Administration: Hampton, VA, 1998.

2. Kvaternik, R. G.; Juang, J.-N.; Bennett, R. L. Exploratory Studies in Generalized Predictive Control for Active Aeroelastic Control of Tiltrotor Aircraft. NASA Technical Memorandum 2000-210552; National Aeronautics and Space Administration: Hampton, VA, 2000.

3. Juang, J.-N.; Phan, M. Q. *Identification and Control of Mechanical Systems*; Cambridge University Press: New York, 2001.

4. Kvaternik, R. G.; Eure, K. W.; Juang, J.-N. Exploratory Studies in Generalized Predictive Control for Active Gust Load Alleviation. NASA Technical Memorandum 2006-214296; National Aeronautics and Space Administration: Hampton, VA, 2006.

5. Brown, R.; Mazza, M.; Murugan, M.; Le, D. Comparison of Generalized Predictive Control Algorithms Using a Full Vehicle Multi-Body Dynamics Model. SAE paper no. 2012-01-1932, SAE 2012; Commercial Vehicle Engineering Congress, Rosemont, IL, 2–3 October 2012.

6. Juang, J.-N. *Applied System Identification*; PTR Prentice Hall: New York, 1994.

7. Bender, E. K. Optimum Linear Preview Control with Application to Vehicle Suspension. *AMSE Journal of Basic Engineering* **1968**, *90*, 213–221.

8. Van der Aa, M. Control Concept for a Semi-Active Suspension With Preview Using a Continuously Variable Damper. Ph.D. Thesis, Eindhoven University of Technology, The Netherlands, 1994.

9. El Madany, M. M.; Abduljabbar, Z.; Foda, M. Optimal Preview Control of Active Suspensions With Integral Constraint. *Journal of Vibration and Control* **2003**, *9*, 1377–1400.

10. Juang, J.-N. *Continuous-Time Bilinear System Identification*; NASA/TM-2003-212646; National Aeronautics and Space Administration: Hampton, VA, September 2003.

11. Brown, R.; Pusey, J.; Murugan, M.; Le, D. Generalized Predictive Control Algorithm of a Simplified Ground Vehicle Suspension System. *SAGE Journal of Vibration and Control* **2002**; paper article no. 1077546312448505.

List of Symbols, Abbreviations, and Acronyms

2-DOF	2 degrees of freedom
AMSAA	U.S. Army Materiel Systems Analysis Activity
ARL	U.S. Army Research Laboratory
ARX	AutoRegressive eXogenous input
ASTR	Advanced Suspension Test Rig
BAA	broad agency agreement
bGPC	bilinear generalized predictive control
d	disturbance inputs
F	control actuator force
GPC	generalized predictive control
HMMWV	High-Mobility Multipurpose Wheeled Vehicle
h_p, h_c	prediction and control horizons
Hz	hertz
km/h	kilometers per hour
L	number of samples used for system identification
m	meter
m, r_c, r_d	number of response outputs, control inputs, disturbance inputs
MR	magnetorheological
MREA	magnetorheological energy absorber
N	newton
OMP	observer Markov parameters
p	order of the ARX model
Q, R	response penalty, control penalty
s	seconds

t	index of current time step
u	control inputs
u(t), y(t), d(t)	vectors of current inputs, outputs, and disturbances at time step *t*
u(t-j) ,y(t-j), d(t-j)	vectors of past inputs, outputs, and disturbances at time step (*t-j*)
u(t+j) ,y(t+j), d(t+j)	vectors of future inputs, outputs, and disturbances at time step (*t+j*)
V	system identification data matrix
VTD	Vehicle Technology Directorate
x_S, x_U	absolute coordinates of sprung and unsprung masses
$\dot{x}_S, \dot{x}_U, \dot{z}_1, \dot{z}_2$	velocity of x_S, x_U, z_1, z_2
$\ddot{x}_S, \ddot{x}_U$	acceleration of x_S, x_U
y	response outputs
$\bar{Y}$	matrix of observer Markov parameters
z_1, z_2	compression of the suspension system and the tire
α_i, β_i δ_i	observer Markov parameters
α_c, β_c, γ_c, δ_c	control law gain matrices
τ, α, β, γ, δ	coefficient matrices in multi-step output prediction equation

NO. OF
COPIES ORGANIZATION

1 (PDF) DEFENSE TECHNICAL INFORMATION CTR
DTIC OCA
8725 JOHN J KINGMAN RD
STE 0944
FORT BELVOIR VA 22060-6218

1 (PDF) DIRECTOR
US ARMY RESEARCH LAB
RDRL CIO LL
2800 POWDER MILL RD
ADELPHI MD 20783-1197

ABERDEEN PROVING GROUND

2 (PDF) DIR USARL
RDRL VTM
D LE
M MURUGAN